communications physics

Article

https://doi.org/10.1038/s42005-024-01861-w

Direct visualization of local magnetic domain dynamics in a 2D Van der Walls material/ferromagnet interface

Check for updates

Joseph Vimal Vas [1,2,6] ✉, Rohit Medwal [3,6], Sourabh Manna [2], Mayank Mishra [2], Aaron Muller [1], John Rex Mohan [4], Yasuhiro Fukuma [4,5], Martial Duchamp [1] ✉ & Rajdeep Singh Rawat [2] ✉

Controlling the magnetic domain propagation is the key to realize ultrafast, high-density domain wall-based memory and logic devices for next generation computing. Two-Dimensional (2D) Van der Waals materials introduce localized modifications to the interfacial magnetic order, which could enable efficient control over the propagation of magnetic domains. However, there is limited direct experimental evidence and understanding of the underlying mechanism, for 2D material mediated control of domain wall propagation. Here, using Lorentz-Transmission Electron Microscopy (L-TEM) along with the Modified Transport of Intensity equations (MTIE), we demonstrate controlled domain expansion with in-situ magnetic field in a ferromagnet (Permalloy, NiFe) interfacing with a 2D VdW material Graphene (Gr). The Gr/NiFe interface exhibits distinctive domain expansion rate with magnetic field selectively near the interface which is further analysed using micromagnetic simulations. Our findings are crucial for comprehending direct visualization of interface controlled magnetic domain expansion, offering insights for developing future domain wall-based technology.

The propagation of domain walls in magnetic materials, which forms the basis of race track memory[1–3] and domain wall logic circuits[4,5], can be stochastic[6,7]. Controlling the propagation of domain walls with both spin currents and/or external magnetic fields[8] is important for the seamless operation of these devices. In order to achieve controlled propagation of magnetic domains, devices based on localized anisotropy, strain modulation[9–11], geometric confinement[6,12], localized heating[13], external magnetic fields, and spin currents[1] have been proposed. These strategies offer unique challenges. For example, in the strain-mediated scheme, a local piezoelectric sublayer introduces strain (through lattice distortion) in the magnetic layer by the application of a local electric field. This method can be cumbersome to fabricate due to complicated growth requirements for epitaxial piezoelectric layers. The switching speed is also a concern (>10 ns switching time of ferroelectric domains[14,15]). Similarly, geometric confinement-based domain wall pinning introduces significant challenges in the fabrication of the ferromagnet as the dimensions need to be restricted to sub-100 nm[16].

Interaction between 2D Van der Waals (VdW) crystals like graphene or hexagonal boron nitride (h-BN) and ferromagnets (FM) can unlock a new array of fascinating phenomena due to the specific nature of these interfaces. Interfacing graphene with Co induces a giant perpendicular magnetic anisotropy (PMA)[17,18]. Capping an FM with graphene exhibits large interfacial Dzyaloshinskii–Moriya interaction (iDMI) emerged from Rashba-type spin–orbit coupling at the graphene/FM interface[19,20]. The iDMI is pivotal for generating, stabilizing, and controlling chiral magnetic structures, with potential applications in memory and logic devices. Localized nanoscale iDMI has been demonstrated to effectively achieve domain wall pinning. Notably, the iDMI can be actively tuned through gate voltage modulation, offering electrical control over the chiral magnetic structures and domain wall motion. Therefore, studying the iDMI in the graphene/ferromagnet interface is crucial. Direct visualization using transmission electron microscopy (TEM) can provide a comprehensive understanding of this phenomenon.

The present study experimentally demonstrates a method for controlling the domain wall motion in a ferromagnetic system by introducing local interfaces between a ferromagnet and 2D material that exhibit significant iDMI[19]. A 5 nm $Ni_{80}Fe_{20}$ with Gilbert's damping factor of 0.0091

[1]Laboratory for in situ and operando Electron Nanoscopy, School of Material Science and Engineering, Nanyang Technological University, Singapore, 9, Singapore. [2]Natural Sciences and Science Education, National Institute of Education, Nanyang Technological University, Singapore, 637616, Singapore. [3]Department of Physics, Indian Institute of Technology, Kanpur, 208016, India. [4]Department of Physics and Information Technology, Kyushu Institute of Technology, Iizuka, 820-8502, Japan. [5]Research Center for Neuromorphic AI hardware, Kyushu Institute of Technology, Kitakyushu, 808-0196, Japan. [6]These authors contributed equally: Joseph Vimal Vas, Rohit Medwal. ✉e-mail: j.vas@fz-juelich.de; martial.duchamp@gmail.com; rajdeep.rawat@nie.edu.sg

has been chosen as the ferromagnet (see Supplementary Note S1 for estimation of the damping factor).

To study the effect of the interface-induced pinning, graphene was transferred to the NiFe thin film. The expansion of the magnetic domains with an external magnetic field near a Gr/NiFe interface is studied to observe the effect of the local iDMI. The magnetic domain mapping requires high spatial resolution near the Gr/NiFe interface, and thus, Lorentz-transmission electron microscopy (L-TEM) is a much-desired tool for such observations[21]. We have performed in-situ domain wall expansion studies using the fringing field of the objective lens of the microscope. The scheme for introducing in-situ magnetic fields for the L-TEM experiments is shown in Fig. 1a. An out-of-plane magnetic field has been applied to the sample using the magnetic field of the objective lens. The in-plane fields required for the in-situ magnetic field effect studies are introduced by small tilts (along x or y direction based on alpha or beta tilt) of the sample holder along with the objective lens field which is in the z-direction. The geometry of NiFe strips used for the study is shown in Fig. 1b. We have discussed the fabrication of the TEM chips used in this study, in Supplementary Note S2. The magnetic field values given in the inset of Fig. 1e are the in-plane magnetic fields for the given objective lens value and tilt conditions.

The initial magnetic domain structure was created by first saturating the NiFe strips through a small alpha tilt (1.9°) and applying a large objective lens field which is gradually reduced to zero. The normalized M_x and M_y of the NiFe layer, calculated from defocused images [described in methods, Modified Transport of Intensity Equations (MTIE), equations (3) and (4)] are given in Fig. 1d (i) and (ii) respectively. The same area was illuminated throughout the measurements with varying in-situ magnetic fields. Distortions were introduced due to the change in focus (objective mini lens) and the objective lens fields used to magnetize the sample. These were compensated by finding a homography transformation matrix[22] to match the distorted image to the in-focus image. A color map of the magnetic signal was then calculated, and the corresponding map for Fig. 1d (i–ii) is given in 1e (i). The different domains present in the NiFe can be easily distinguished after the MTIE calculations. The red contrast seen at the edges of the NiFe strip (in Fig. 1e) is the measurement error. This is caused by the improper matching between the in-focus and out-of-focus images due to the Fresnel fringes at the sample edges produced by the defocusing.

Results

In-situ magnetization studies of NiFe

The spatial evolution of magnetization of NiFe was conducted by applying an external field as shown in Fig. 1e. At 0 Oe, the blue domains (along ~−x direction) and the green domains (along ~+x direction) occupy almost equal area on the NiFe strip. The magnetization of the NiFe strip also displays magnetic ripple contrast, indicating the polycrystalline nature of NiFe layer[23]. The direction of the electron beam is along z-axis as shown in Fig. 1a. The in-situ magnetic field along the x-direction was applied by tilting the TEM chip (alpha tilt) by 1.9° and gradually increasing magnetic field by the objective lens field of the TEM using the free lens controller (co-ordinate system and tilt directions with respect to the holder are shown in Fig. 1a). The shrinking of the blue domains with increasing in-plane external field is clearly observed. At 80.5 Oe, the strip is almost completely magnetized along the direction of the green domains (which is the direction of the in-plane field induced by the sample tilt), and the NiFe strip effectively becomes a single domain with in-plane magnetization. The presence of the magnetic ripple contrast arising from local variation in magnetization due to the presence of grains may have increased the saturation field which is comparable with NiFe wires reported in literature[24,25]. The raw images used for

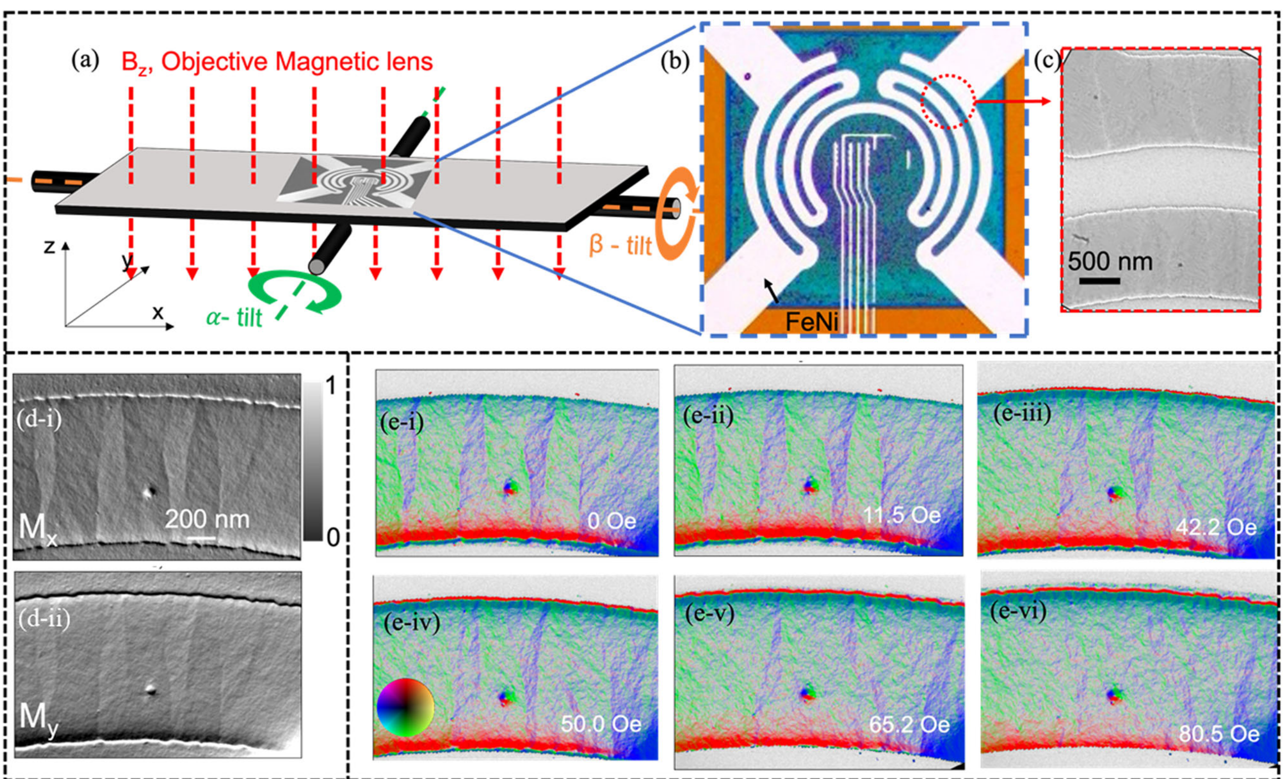

Fig. 1 | In-situ TEM experiments on NiFe strips. **a** Schematic of the sample holder and the mechanism for introducing in-plane fields. In-plane magnetic fields are generated using α and β tilt of the holder in a controlled out-of-plane objective lens field. **b** Geometry of the NiFe strips deposited on the MEMS chip. **c** Out-of-focus TEM image of the NiFe strip showing domain walls. **d** (i) M_x and (ii) M_y of the initial magnetization. **e** Color map of the in-plain domains in the NiFe strips with an in-situ magnetic field applied along x-direction from (i–vi) 0 to 80.5 Oe.

the calculation are given in supplementary information, Fig. S6 in Supplementary Note 4.

Domain wall motion at the Gr/NiFe interface

The next step is to study the domain wall propagation in the vicinity of the Gr/NiFe interface. The preparation of the Gr/NiFe interface is discussed in Supplementary Note S3. The location of the graphene flake and an image of the Gr/NiFe interface taken in the Lorentz mode are shown in Fig. 2a, b. The quality of the Gr/NiFe interface was studied using the cross-section TEM after the experiments were done, are shown in Supplementary Note S3. The thickness of the graphene was ~2 nm indicating about 10 layers. The TEM of graphene showed 6-member carbon rings (refer to Fig. S4 in Supplementary Information) with the absence of atomistic defects. No amorphous layer was observed between graphene and the polycrystalline NiFe, as shown in Fig. S5 of Supplementary Information, indicating a clean VdW/FM interface. The DMI interaction between the NiFe and graphene is short-ranged to <3 nm of the interface[26]. Any small amorphous deposits between the two layers can reduce the strength of the interaction, and thus, the influence on the domain wall dynamics becomes substantially low.

The initial domain wall configuration was produced by introducing both alpha (±5°) and beta (±5°) tilts, saturating the magnetization using a large objective field and subsequently reducing the magnetic field and the tilts back to 0. The calculated magnetization overlayed onto the in-focus L-TEM images near the Gr/NiFe interface when magnetized along $+x$ and $-x$ directions are given in Fig. 2c, d(i–v) respectively. The magnetic field values given in Fig. 2c, d are the effective in-plane magnetic fields acting on the sample. The domain walls outside graphene are marked using a white arrow, while the domain walls under graphene are marked using a yellow arrow. The defocused LTEM images acquired for different field conditions are given in Supplementary Note S4.

The initial magnetization conditions, characterized by the presence of one domain wall located outside the graphene area and another beneath the graphene, were similar for both field sweeps. The domain walls were subsequently moved by the in-situ magnetic fields generated by the objective lens field and the alpha tilt. The field direction was set to move the domain wall to the right ($+x$ direction, 1° alpha tilt), as shown in Fig. 2a(i–v). Increasing the magnetic field to 15 Oe moved the domain wall in uncovered NiFe to the right while the domain wall under graphene remained stationary. Increasing the field even further to 25 Oe deformed the domain wall under the graphene region slightly, but the uncovered domain wall moved further along the NiFe strip. Thus, there is an asymmetry in the motion of the domain walls with magnetic fields under and outside the graphene which is observed for both $+x$ and $-x$ directions. For the $-x$ field sweep, the domain under the graphene switched instantaneously after the in-situ magnetic field of 30 Oe. Similar to the measurements on the NiFe strip (Fig. 1e), magnetic ripple contrast from the polycrystalline NiFe grains of varying magnetization has been observed in this case as well.

Effect of different magnetic energies

The asymmetry in the motion of the NiFe domain wall under and outside graphene is due to the local modification in the energy density landscape induced by the Gr/NiFe interface. The presence of DMI[19] and PMA[17] at graphene/FM interfaces has been demonstrated using first principle calculations and spin-polarized low-energy electron microscopy (SPLEEM). Considering these possible interfacial effects, the total magnetic energy density of the NiFe strip in the presence of the Gr/NiFe interface can be expressed as follows,

$$E_{Total} = E_{Zeeman} + E_{\text{exchange}} + E_{magnetostatic} + E_{PMA} + E_{DMI} \tag{1}$$

In the presence of external magnetic fields, the sizes of the domains are determined in such a way that the total energy of the NiFe strip is minimized. Hence, we carried out a micromagnetic simulation in MuMax3[27] following the energy minimization routine to understand the possible effect of iDMI and PMA at the Gr/NiFe interface. We model a similar NiFe strip, partially covered with a graphene flake as observed in the L-TEM. The presence of graphene is implicitly modeled by defining a finite DMI and/or PMA only in that particular region which represents the area under the graphene. Detailed methodology of micromagnetic simulation is discussed in the supplementary information, Supplementary Note S5.

We conducted an L-TEM study with a finer in-situ magnetic field step size of 0.25 Oe to compare the results with micromagnetic simulations. The rate of domain expansion has been quantified by calculating the domain expansion factor, ϵ which was defined as,

$$\epsilon = \frac{A_{Domain1}}{A_{Domain1} + A_{Domain2}} \tag{2}$$

where $A_{(Domain\ 1\ (2)}$ is the area under the domain 1 (2).

The domain expansion factor ϵ under graphene and outside graphene is given in the Fig. 3(a-i), for each value of the in-situ magnetic field when the domain expands. Note that, both domains are partially covered by the graphene flake. The domain expansion rate, as a function of the magnetic field, is staggered up to around 25 Oe. This is possibly due to the presence of geometrical defects at the edges, which act as the pinning sites. The entire plot is given in Supplementary Information, Supplementary Note S4. We observe from Fig. 3a that the slope of the domain expansion rate is a linear function of the magnetic field. The rate of domain expansion is smaller at the

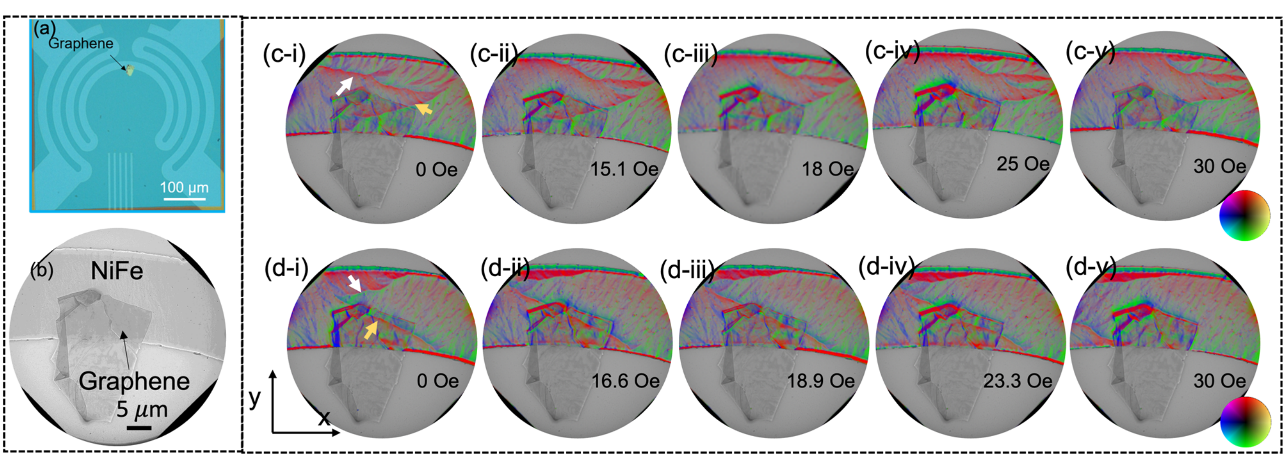

Fig. 2 | Domain wall propagation with magnetic field in the Gr/NiFe device. **a** Image of the TEM chip showing the location of the Gr/NiFe interface, **b** high-resolution TEM image of the Graphene placed on permalloy. Domain wall expansion near the Gr/NiFe interface with in-situ magnetic fields along the **c** (i–v) +x field sweep and **d** (i–v) −x field sweep.

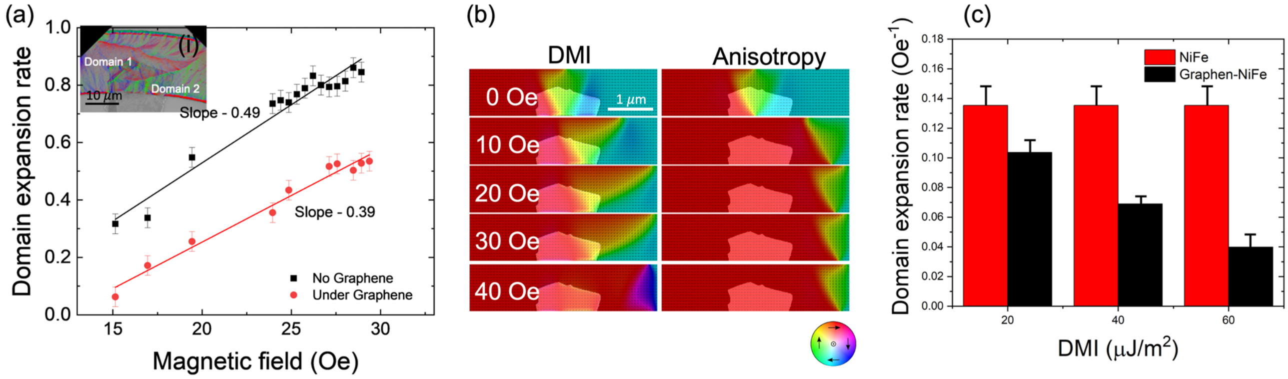

Fig. 3 | Comparison of experimental domain wall expansion in Gr/NiFe with micromagnetic simulations. a Domain expansion rate with the magnetic field when the domain expands, the inset (i) shows domain 1 and domain 2 mentioned in Eq. 2 along with the initial domain configuration. The error bars are calculated from the width of the domain wall measured from the defocused images. **b** Simulated expansion of domain within the plane magnetic field with anisotropy (K_u = 4.021 kJ/m^3) and DMI (2.35 mJ/m^2) and **c** simulated rate of domain wall expansion for different DMI values (20–60 μJ/m^2). The error bars represent the standard deviation of the data extracted from the simulation results.

Gr/NiFe interface (black circles) as compared to its counterpart outside the Gr/NiFe interface (red circle). We have estimated the slopes as 0.0485 Oe^{-1} (from red circles) and 0.0388 Oe^{-1}(from black circles) for the area outside and within the Gr/NiFe interface, respectively. Hence, we conclude that the presence of graphene indeed slows down or "brakes" the domain expansion in NiFe.

The braking of the domain expansion can occur only if the mobility of the domain wall is different under graphene compared to outside the graphene area. A simple theoretical estimate of the domain wall mobility can be obtained using the formula, $\mu = \gamma\Delta/\alpha$, where γ is the gyrometric ratio, Δ is the domain wall width, and α is the Gilbert's damping factor. The Gilbert's damping factor for NiFe/Gr is higher than the bare NiFe films as shown in the FMR measurements in Supplementary Information, S1. The relative domain wall width measured from the Lorentz TEM images shows that the width reduces under graphene, as shown in Supplementary Note, S6. Thus, the mobility of the domain wall under graphene is relatively lower than the bare NiFe layer, which could have resulted in the braking effect observed.

We have performed micromagnetic simulations to understand the origin of such a "braking effect" and reduced mobility on domain wall expansion induced by the Gr/NiFe interface. It should be noted that a fully quantitative agreement between the experimental results and simulation could be hardly obtained because of the inevitable mismatch between the simplified micromagnetic model and the real experimental conditions. However, from the qualitative agreement between our experiment and the simulation results, we explain the underlying phenomena. We have first defined a domain wall which is partly Bloch and partly Neel type, at the center of a rectangular NiFe strip. In addition, we introduced PMA and DMI locally at the Gr/NiFe interface and varied their strength to observe the domain wall motion under the influence of different external magnetic fields. A parametric study with PMA has been performed with K_u ranging from 0.4 to 40.21 kJ/m^3 and iDMI strength from 2.3 to 2.5 mJ/m^2 at the Gr/NiFe interface to observe the possible pinning effect (due to roughness, see Supplementary Note S7) on the domain wall as observed experimentally. This is given in Supplementary Note S5. Softly pinned domain walls were observed with a PMA, K_u = 4.021 kJ/m^3, or an iDMI strength of 2.35 mJ/m^2 at the Gr/NiFe interface. These are investigated in detail and are shown in Fig. 3b. Even though the domain structure was initialized with a vertical domain wall across the width of the NiFe strip (Supplementary Information, Fig. S9 (a)), the introduction of PMA and iDMI at the interface changed the shape of the domain wall similar to those observed experimentally. However, the introduction of PMA at the Gr/NiFe interface did not exhibit any pinning effect of domain walls, whereas the iDMI at the interface significantly hindered the domain expansion exhibiting the "braking effect". This indicates that the "braking effect" experimentally observed, is because of the interfacial DMI at the Gr/NiFe interface.

The DMI value of 2.35 = mJ/m^2 used in the simulation [shown in Fig. 3c] is comparable with values observed by Yang et al.[19] and appears higher than other experimental measurements[28] on Gr/NiFe interfaces. These experiments report DMI values within the range of 60 μJ/m^2, with multiple graphene layers reducing the interfacial DMI. This could be because the effect of the polycrystalline nature of our NiFe film was not considered in this simulation. To verify this, we carried out micromagnetic simulations with 40 nm grain size and 10% variation in M_s using the *in-built* Voronoi Tessellation functionality of MuMax[3 27] (which was used to obtain Fig. 3a) with an additional iDMI value in the range of 0–60 μJ/m^2. The domain expansion rate was calculated for different iDMI values and is presented in Fig. 3c. There is a clear reduction in domain expansion rate with increasing iDMI, and with an iDMI value of 60 μJ/m^2 the domain expansion rate was comparable to the experimentally observed values. Thus, we conclude that the soft pinning of domain walls observed in the in-situ L-TEM study near the Gr/NiFe interface was due to iDMI introduced at the interface. This could be used to spatially stifle the expansion of domains to control the domain wall propagation on demand.

Discussion

We demonstrate that introducing Graphene onto NiFe can reduce the domain expansion rate with a magnetic field. Comparison between the Lorentz TEM imaging on NiFe strips with a local Gr/NiFe interface with in-situ magnetic fields with the micromagnetic simulations indicates the reduction in domain wall expansion rate was due to the iDMI introduced by the Gr/NiFe interface. The iDMI strength has been estimated to be around 60 μJ/m^2 based on the simulations considering the variation of dipolar interaction and exchange interaction across the grains to incorporate the microcrystals observed in the L-TEM studies. Spatially arranged interfaces along the length of an FM strip can, therefore, control the expansion of domains which is the key to domain wall memory systems like domain wall logic circuit[5,13,29] and racetrack memory[1,3,30] schemes.

Methods

Lorentz transmission electron microscopy (LTEM)

The LTEM imaging was done in a double-corrected JEOL ARM 300 microscope in Lorentz mode operated at 300 kV and the objective lens turned off. The probe corrector was turned off as well in this mode, and the image corrector was tuned to obtain a spatial resolution of ~1 nm using a special gold sample of appropriate particle size. For the LTEM imaging, the sample was moved through the focus using the objective mini lens of the image corrector. NiFe devices with and without graphene are prepared on a MEMS chip with a 200 nm thick silicon nitride window which was compatible with a Hennyz TEM holder[21]. The fabrication of the MEMs chips and the transfer of the graphene is discussed in Supplementary Information S2 and S3. The transfer protocol was optimized using high-resolution transmission electron microscopy to ensure a clean interface between the NiFe and Graphene.

Modified transport of intensity equations

The magnetization mapping of the NiFe sample changes the phase of the electron wave passing through and is observed in Lorentz mode when the image is out of focus. The magnetization of the NiFe strip is calculated using the modified transport of intensity equation (MTIE) based on the difference in intensity between the in-focus and out-of-focus images[31]. The equations for the same are given below,

$$\phi(r) = F^{-1}\left[F\left(k_z\delta_z I/I\right)/k_\perp^2\right] \tag{3}$$

$$tB = \frac{\hbar}{e}\left[n_z \times \Delta\phi\right] \tag{4}$$

Where $\phi(r)$ is the phase change in the electron wave introduced by the sample, F and F^{-1} denotes the Fourier and inverse Fourier transform, k_z is the propagation constant of the electron wave in vacuum, $\delta_z I$ represents the change in intensity with defocus, $k_\perp$ is the frequency vector in Fourier space, t is the thickness of the sample, B is the magnetization, $\hbar$ is reduced plank constant, e is the electronic charge and n_z is the unit vector along z direction. Equation 2 has a singularity when $k_\perp$ becomes zero, and a low pass filter is used to get rid of this. The electron phase, $\phi(r)$ thus calculated using L-TEM can only provide a relative value for the magnetization of the samples. The code used for the calculation has been uploaded on Github[32].

Micromagnetic simulations

The micromagnetic simulation was performed using the open-source software MuMax[3 27] on a rectangular strip of 2048 nm × 512 nm × 10 nm size, discretized into rectangular cells of 2 nm × 2 nm × 10 nm. NiFe material parameters derived from the analysis of FMR spectra were used for the simulation. The exchange constant of NiFe was obtained from the literature as $A_{ex} = 13$ pJ/m. The Gr/NiFe interface on the NiFe strip was later defined by importing an image mask of the Graphene patch, scaled in accordance with the dimension of the NiFe strip. The spatial distribution of magnetic moments in each cell was initialized as a two-domain configuration where, the magnetization at the left and right halves are defined along the x-axis, facing each other (Supplementary Information, Fig. S9a). The domain wall (DW) at the middle of the NiFe strip was defined as a mixed state of Bloch wall and Néél wall. DMI and PMA were explicitly defined at the Gr/NiFe interface using the built-in MuMax functions. In each simulation, the final magnetization configuration in the NiFe strip was obtained after relaxing the magnetization to the minimum energy state in the presence of an external magnetic field, followed by solving the Landau–Lifshitz–Gilbert equation. For a detailed discussion on micromagnetic simulation, please see the Supplementary Information, Section S5.

Data availability

The data are available from the corresponding author upon reasonable request.

Received: 25 March 2024; Accepted: 5 November 2024;
Published online: 19 December 2024

References

1. Parkin, S. S., Hayashi, M. & Thomas, L. Magnetic domain-wall racetrack memory. *Science* **320**, 190–194 (2008).
2. Zhao, W. S. et al. Magnetic domain-wall racetrack memory for high density and fast data storage. in *2012 IEEE 11th International Conference on Solid-State and Integrated Circuit Technology* 1–4 https://doi.org/10.1109/ICSICT.2012.6466687 (2012).
3. Parkin, S. & Yang, S.-H. Memory on the racetrack. *Nat. Nanotechnol.* **10**, 195–198 (2015).
4. Luo, Z. et al. Current-driven magnetic domain-wall logic. *Nature* **579**, 214–218 (2020).
5. Allwood, D. A. et al. Magnetic domain-wall logic. *Science* **309**, 1688–1692 (2005).
6. Akerman, J., Muñoz, M., Maicas, M. & Prieto, J. L. Stochastic nature of the domain wall depinning in permalloy magnetic nanowires. *Phys. Rev. B* **82**, 064426 (2010).
7. Hayward, T. J. Intrinsic nature of stochastic domain wall pinning phenomena in magnetic nanowire devices. *Sci. Rep.* **5**, 13279 (2015).
8. Jacot, B. J. et al. Control of field- and current-driven magnetic domain wall motion by exchange bias in Cr2O3/CoPt trilayers. *Phys. Rev. B* **106**, 134411 (2022).
9. Zhang, J. et al. Spontaneous formation of ordered magnetic domains by patterning stress. *Nano Lett.* **21**, 5430–5437 (2021).
10. Yu, G. et al. Strain-driven magnetic domain wall dynamics controlled by voltage in multiferroic heterostructures. *J. Magn. Magn. Mater.* **552**, 169229 (2022).
11. Rana, B. & Otani, Y. Towards magnonic devices based on voltage-controlled magnetic anisotropy. *Commun. Phys.* **2**, 90 (2019).
12. Bogart, L. K., Eastwood, D. S. & Atkinson, D. The effect of geometrical confinement and chirality on domain wall pinning behavior in planar nanowires. *J. Appl. Phys.* **104**, 033904 (2008).
13. Mazo-Zuluaga, J., Velásquez, E. A., Altbir, D. & Mejía-López, J. Controlling domain wall nucleation and propagation with temperature gradients. *Appl. Phys. Lett.* **109**, 122408 (2016).
14. Parsonnet, E. et al. Toward intrinsic ferroelectric switching in multiferroic BiFeO3. *Phys. Rev. Lett.* **125**, 067601 (2020).
15. Ghosh, S. et al. Current-driven domain wall dynamics in ferrimagnetic nickel-doped Mn4N films: very large domain wall velocities and reversal of motion direction across the magnetic compensation point. *Nano Lett.* **21**, 2580–2587 (2021).
16. Groves, T. R. et al. Maskless electron beam lithography: prospects, progress, and challenges. *Microelectron. Eng.* **61–62**, 285–293 (2002).
17. Blanco-Rey, M. et al. Large perpendicular magnetic anisotropy in nanometer-thick epitaxial graphene/CO/heavy metal heterostructures for spin–orbitronics devices. *ACS Appl. Nano Mater.* **4**, 4398–4408 (2021).
18. Yang, H. et al. Anatomy and giant enhancement of the perpendicular magnetic anisotropy of cobalt–graphene heterostructures. *Nano Lett.* **16**, 145–151 (2016).
19. Yang, H. et al. Significant Dzyaloshinskii–Moriya interaction at graphene–ferromagnet interfaces due to the Rashba effect. *Nat. Mater.* **17**, 605–609 (2018).
20. Blanco-Rey, M., Bihlmayer, G., Arnau, A. & Cerdá, J. I. Nature of interfacial Dzyaloshinskii-Moriya interactions in graphene/Co/Pt(111) multilayer heterostructures. *Phys. Rev. B* **106**, 064426 (2022).
21. Tyukalova, E. et al. Challenges and applications to operando and in situ TEM imaging and spectroscopic capabilities in a cryogenic temperature range. *Acc. Chem. Res.* **54**, 3125–3135 (2021).
22. Zhou, Q. & Li, X. STN-homography: direct estimation of homography parameters for image Pairs. *Appl. Sci.* **9**, 5187 (2019).
23. Hamada, K., Chimura, M., Arita, M., Ishida, I. & Okada, A. Magnetic microstructure of NiFe/Cu/NiFe films observed by Lorentz microscopy. *J. Electron Microsc.* **48**, 595–600 (1999).
24. Cowburn, R. P., Allwood, D. A., Xiong, G. & Cooke, M. D. Domain wall injection and propagation in planar Permalloy nanowires. *J. Appl. Phys.* **91**, 6949 (2002).
25. Goncharov, A. V. et al. In-plane anisotropy of coercive field in permalloy square ring arrays. *J. Appl. Phys.* **99**, 08Q508 (2006).
26. Dhiman, A. K. et al. Thickness dependence of interfacial Dzyaloshinskii-Moriya interaction, magnetic anisotropy and spin

waves damping in Pt/Co/Ir and Ir/Co/Pt trilayers. *J. Magn. Magn. Mater.* **519**, 167485 (2021).
27. Vansteenkiste, A. et al. The design and verification of MuMax^3. *AIP Adv.* **4**, 107133 (2014).
28. Chaurasiya, A. K. et al. Direct observation of unusual interfacial Dzyaloshinskii-Moriya interaction in graphene/NiFe/Ta heterostructures. *Phys. Rev. B* **99**, 035402 (2019).
29. Allwood, D. A. et al. Submicrometer ferromagnetic NOT gate and shift register. *Science* **296**, 2003–2006 (2002).
30. Zhang, X. et al. Skyrmion-skyrmion and skyrmion-edge repulsions in skyrmion-based racetrack memory. *Sci. Rep.* **5**, 7643 (2015).
31. Volkov, V. V. & Zhu, Y. Lorentz phase microscopy of magnetic materials. *Ultramicroscopy* **98**, 271–281 (2004).
32. Vas, J. V. & Duchamp, M. *Modified-Transport-of-Intensity-for-Lorentz-Microscopy*. https://github.com/jvvas/Lorentz-Image-Processing (2023).

Acknowledgements
S.M. acknowledges the support from the NTU-Research Scholarship (NTU-RSS). R.S.R. acknowledges the Ministry of Education, Singapore, for the support through MOE Tier 2 Grant, ARC-1/17 RSR (MOE2017-T2-2-129) and MOE Tier 1 Grant RG 76/22. Any opinions, findings, conclusions, or recommendations expressed in this material are those of the author(s) and do not reflect the views of the Ministry of Education, Singapore.

Author contributions
J.V.V. and R.M. conceived the idea. S.M. performed the micromagnetic simulations. M.M. conducted the data analysis and associated statistics, and A.M. fabricated the chips and the 2D devices. J.R.M. and Y.F. deposited the NiFe and FMR measurements. M.D., J.V.V., and R.M. did the L-TEM measurements. M.D. and J.V.V. created the MTIE-based reconstruction code. J.V.V. and S.M. prepared and polished the draft with inputs from all the authors. R.M., R.S.R., and M.D. supervised the project.

Competing interests
The authors declare no competing interests.

Additional information
Supplementary information The online version contains supplementary material available at https://doi.org/10.1038/s42005-024-01861-w.

Correspondence and requests for materials should be addressed to Joseph Vimal Vas, Martial Duchamp or Rajdeep Singh Rawat.

Peer review information *Communications Physics* thanks Duck-Ho Kim and the other, anonymous, reviewer(s) for their contribution to the peer review of this work.